Polymer Chemistry

Accepted Manuscript

This is an *Accepted Manuscript*, which has been through the Royal Society of Chemistry peer review process and has been accepted for publication.

Accepted Manuscripts are published online shortly after acceptance, before technical editing, formatting and proof reading. Using this free service, authors can make their results available to the community, in citable form, before we publish the edited article. We will replace this *Accepted Manuscript* with the edited and formatted *Advance Article* as soon as it is available.

You can find more information about *Accepted Manuscripts* in the Information for Authors.

Please note that technical editing may introduce minor changes to the text and/or graphics, which may alter content. The journal's standard Terms & Conditions and the Ethical guidelines still apply. In no event shall the Royal Society of Chemistry be held responsible for any errors or omissions in this *Accepted Manuscript* or any consequences arising from the use of any information it contains.

ROYAL SOCIETY OF CHEMISTRY

www.rsc.org/polymers

A Poly(polyoxometalate)-*b*-Poly(hexanoic acid) Block Copolymer: Synthesis, Self-Assembled Micelles and Catalytic Activity

Wen-Ke Miao, Ang Yi, Yu-Kun Yan, Li-Jun Ren, Da Chen, Chun-Hong Wang, Wei Wang*

[1]Center for Synthetic Soft Materials, Key Laboratory of Functional Polymer Materials of the Ministry of Education, Institute of Polymer Chemistry, Nankai University, Tianjin 300071, China.

[2]Collaborative Innovation Center of Chemical Science and Engineering (Tianjin), Tianjin 300071, China.

*E-mail: weiwang@nankai.edu.cn.

A hybrid block copolymer (H-BCP) composed of a poly(polyoxometalate) (poly(POM)) block and a poly(6-norbornene-hexanoic acid) (poly(COOH)) block was prepared by sequential addition of two norbornene monomers containing a POM cluster and a carboxyl as side groups via ring-opening metathesis polymerization (ROMP). Because the 5833 Da molecular weight of the POM-containing monomer is much higher than 277 Da of the carboxyl-containing monomer, the designed H-BCP has degrees of polymerization $DP = 5$ for the poly(POM) block and $DP = 200$ for the poly(COOH) block. Thus, the H-BCP not only has differences in chemical structure and property but also asymmetries in molecular weight and length. In acetonitrile, it self-assembles into hybrid micelles with a thin shell of the poly(POM) block and a core of the poly(COOH) block. The micelles form thin films in which the micelles pack into a hexagonal pattern driven by attractive capillary forces between the micelles. Meanwhile, they H-BCP exhibits good catalytic activity. The H-BCP may become an important candidate for producing hybrid materials with good processability and ductility of the polymer components, and good functionality of the POM clusters.

Introduction

Rapid advances in science and technology demand materials with a variety of desired functions. Organic-inorganic hybrid materials are an important candidates with tailorable performance and functionality.[1] Over the past decades, functional hybrid materials have been widely used in many fields including fuel/solar cells,[2,3] optics and photonics,[4] biomedical chemistry,[5] magnetic nanomaterials,[6] photochromic materials,[7] etc. Organic polymer-based hybrid materials have become increasingly important because they have good processability, attractive mechanical performances and interesting functionalities.[8,9] In contrast to traditional composites, successful hybrid materials are nanoscale composites with an emphasis on nanosized two-phase structures of polymers and inorganic components. This allows optimization of their functions and performances. Thus, a deliberate component selection and a careful design of molecular and supramolecular hybrid structures are required.

Inorganic clusters have definite physical structures and sizes, diverse and complex chemical structures and compositions, and unique and attractive properties and functions.[10] They have become increasingly important components for the generation of polymer-based hybrid materials.[11,12] Polyoxometalates (POMs) are a class of inorganic metal-oxygen anionic and nanosized clusters of early transition metals.[13,14] Their structural and chemical diversity and attractive functions make them be excellent inorganic building blocks for the construction of organic-inorganic hybrid functional materials. Covalent incorporation of POM clusters into polymers is an attractive strategy to create novel POM-polymer hybrid materials with good processability and mechanical performances of polymers and functionalities of POM clusters.[15–37] Unfortunately, it remains difficult to carefully control the macromolecular structures of the POM-polymer hybrids. Meanwhile, poor solubility of these hybrids in most solvents makes further characterizations of their chemical structures and molecular weights difficult. Thus, studies of their physical structures and properties as well as potential applications are seriously impeded.

It is well-known that most POM clusters are chemically active. Thus, this chemical activity can strongly affect the synthesis of the polymers-based hybrids with

controllable macromolecular structures and molecular weights. In 2009 we started the project aiming at designing and synthesizing hybrids that are composed of one POM cluster and one or two polymer chains.[27–30,34–36] The first hybrid polymer is composed of a Wells-Dawson POM cluster and a polystyrene chain.[27] It was synthesized via atom transfer radical polymerization (ATRP) from a POM-containing macroinitiator. Because its macromolecular structure and molecular weight were well controlled, the hybrid polymer exhibited very interesting self-assembled structures in solution.[27–30] Soon after, Rieger, Hasenknopf, Lacôte, and coworkers applied a similar method to prepare POM-poly(*N*,*N*-diethylacrylamide)[31,32] or POM-PS[33] hybrids via reversible addition–fragmentation chain transfer (RAFT) radical polymerization and also studied their aggregation in water. We also used other methods, such as click[34] and esterification[35,36] reactions, to combine POMs and polymers together. Importantly, our recent studies show that such POM-polymer hybrids can self-assemble into nano-enhancers to tailor the performances of the nanocomposites.[36]

Recently, we have achieved a new milestone in our quest to advance the polymerization of a POM-containing monomer to generate linear poly(polyoxometalate)s (poly(POM)s), in which the POM clusters as side groups regularly distribute along the polymer backbones.[37] In that study, we first prepared a POM-containing norbornene monomer and then produced linear poly(POM)s with well-defined structures and high molecular weights through exploitation of living ring-opening metathesis polymerization (ROMP). More attractively, the linear poly(POM)s have good catalytic performances in solution and form good films from the solution. These findings not only pave the way for incorporating POM clusters into polymers, but also offer a competitive strategy for developing novel functional hybrid materials.

Block copolymers (BCPs) exhibited remarkable structural diversity of supramolecular aggregates in solution or microphase-separated domains in bulk.[38,39] Interestingly, many hybrid BCPs have been prepared, and their supramolecular aggregates or microphase-separated domains have been utilized to construct functional hybrid materials.[2] Influenced by past achievements and considering our

capability in managing the living ROMP of the POM-containing norbornene monomer,[37] we synthesized the first linear hybrid BCP (H-BCP) composed of an inorganic linear poly(POM) block and an organic polynorbornene block by sequential addition of a POM-containing norbornene and an organic norbornene monomers via living ROMP. We then studied its self-assembled structures in solution as well as in thin films. Meanwhile, we appraised catalytic function of the hybrid BCP in solution.

Experimental

Materials: *cis*-5-norbornene-*exo*-2,3-dicarboxylic anhydride (96%), 12-aminolauric acid, 6-aminocaproic acid, and ethyl vinyl ether (99%, EVE) were purchased from J&K and used directly. Grubbs catalyst, 2nd generation, was purchased from Sigma-Aldrich and its 3rd generation was synthesized following a procedure reported in literature.[40] The trivanadium-substituted Wells-Dawson-type polyoxotungstate $[(Bu_4N^+)_6H_3(P_2W_{15}V_3O_{62})^{9-}]$ was synthesized following a typical experimental procedure.[41,42] *N,N*-dimethylformamide (DMF) and acetonitrile (ACN) were dried and freshly distilled. All other chemicals were from commercial sources and used as received.

Characterizations: ^{1}H NMR (400 MHz) spectra, ^{13}C NMR (100 MHz) and ^{31}P NMR (162 MHz) spectra were recorded on a Varian UNITY plus-400 spectrometer in dimethylsulfoxide-*d*6 (DMSO-*d*6) with tetramethylsilane (TMS) as an internal reference. FT-IR spectra were taken on a FT-IR spectrometer (Bio-Rad FTS-135) sampled with KBr pellet samples. Size exclusion chromatography (SEC) was performed in DMSO (containing 0.1% LiBr) at a flow rate of 0.2 mL/min at 30 °C on a Viscotek 270max system equipped with a GPCmax isolated pump, an autosampler, an A6000M column, a VE3580 RI detector, a 270max light scattering detector and a viscometer, with narrow dispersed polystyrenes (PS) and poly(ethylene oxide)s (PEO) as standards. Transmission electron microscopy (TEM) was performed using a field emission transmission electron microscopy FEI Tecnai G2 F20 operating at an acceleration voltage of 200 kV. The High Performance Liquid Chromatography (HPLC) analysis was performed on Agilent 1200 system with 1200 diode-array

detector and 1200 quaternary pump with degasser. A reversed-phase column (200 mm×4.6 mm ID) packed with Kromasil C18 (5 mm) was used for chromatographic analysis. The mobile phase was acetonitrile–H_2O (20:80, v/v) in the first three minutes and acetonitrile–H_2O (60/40, v/v) in the next 9 min with flow rate of 1 mL/min. (TEM)

Synthesis of Monomer 1. **1** was synthesized according to our recent report.[37]

Synthesis of Monomer 2. **2** was synthesized according to the literature.[37,43,44] A mixture of 492.5 mg (3.0 mmol, 1 eq) of *cis*-5-norbornene-*exo*-2,3-dicarboxylic anhydride and 432.9 mg (3.3 mmol, 1.1 eq) of 6-aminocaproic acid was boiled in glacial acetic acid (20 mL) for 6 hours. After evaporation of the solvent, the residue was dissolved in 50 mL of ethyl acetate, then washed with 50 mL of distilled water for 3 times to remove the 6-aminocaproic acid. The organic phase was dried over anhydrous sodium sulfate, and evaporated to give a white solid (771.1 mg, 2.8 mmol，93 %). ^{1}H NMR (Fig. S2 in the ESI†) (400 MHz, DMSO): δ = 12.08 (br, 1H, COO<u>H</u>), 6.31 (s, 1H, C<u>H</u>=C<u>H</u>), 3.33 (t, *J*=7.2 Hz, 2H, NC<u>H</u>$_2$), 3.09 (s, 2H, COC<u>H</u>), 2.68 (s, 1H, CH=CHC<u>H</u>), 2.17 (t, *J*=7.3 Hz, 2H, C<u>H</u>$_2$CO), 1.99 (s, 1H, C<u>H</u>$_2$CH), 1.10~1.52 (m, 9H, C<u>H</u>$_2$). ^{13}C NMR (Fig. S3 in the ESI†) (100 MHz, DMSO): δ =177.64, 174.37, 137.61, 47.21, 44.42, 42.33, 37.71, 33.43, 26.91, 25.83, 23.98.

Synthesis of the hybrid block copolymer (H-BCP). The designed H-BCP is poly(POM)$_5$-*b*-poly(COOH)$_{200}$. It was synthesized *via* ROMP by sequential addition of **1** to obtain poly(POM)$_5$ and then **2** to obtain poly(POM)$_5$-*b*-poly(COOH)$_{200}$. In a vial charged with 121.2 μL of dry DMF solution of **1** (70.7 mg, 1.2×10^{-2} mmol, 0.1 mmol/mL), 48.5 μL of dry DMF solution of Grubbs' 3rd catalyst (2.1 mg, 0.05 mmol/mL DMF) was added under vigorous stirring. After 1 hour, 25.7 μL of the polymerization mixture was withdrawn with a syringe and quenched with 0.1 mL of EVE for further characterization. To the remaining polymerization mixture was added **2** (114.1 mg, 0.41 mmol, 1.0 mmol/mL) in dry DMF (411.4 μL) solution which was left to stir until approx. 100% conversion (1 hour as determined by ^{1}H NMR). The copolymer solution was then quenched with EVE (0.2 mL), and left to stir for 10 min before precipitation into a large excess of Et_2O and dried under vacuum until constant

weight. ^{1}H NMR (Fig. S5 in the ESI†) (400 MHz, DMSO-d_6): δ = 11.89 (s, COOH), 7.47 (br, CONH), 5.33-5.74 (m, HC=CH, CCH_2O), 3.36-3.41 (m, CH_2NCO), 3.18 (m, $NCH_2CH_2CH_2CH_3$), 3.03 (br, NCOCH), 2.56-2.67 (m, $CH_2CHCH{=}C$), 2.16 (br, CH_2COOH), 1.95 (br, $CH_2CHCH{=}$), 1.58 (br, $NCH_2CH_2CH_2CH_3$), 1.33 (q, J = 7.1 Hz, $NCH_2CH_2CH_2CH_3$), 1.38-1.50, 1.07-1.28 (m, CH, CH_2), 0.94 (t, J = 7.0 Hz, $NCH_2CH_2CH_2CH_3$). ^{31}P NMR (162 MHz, DMSO-d_6): δ = −7.63 (s, P1), −13.76 (s, P2). FT-IR (KBr pellet, Fig. 1D): 3287 (O–H *str*), 2932, 2855 (C–H *str*), 1763, 1701 (C=O *str*), 1539 (N–H *str*), 1088, 951, 911, 820 (P–O *str*, W–O *str*, W–O–W *str*). The ^{1}H NMR and ^{31}P NMR spectra of poly(POM_5) and H-BCP are given in Figs. S4 and S5 and in Fig. 1C. The FT-IR spectrum of the H-BCP is given in Fig. 1D.

Catalytic oxidation of tetrahydrothiophene (THT). In a typical reaction, the H-BCP catalysts (10.0 mg, 0.1 μmol of the poly(POM)$_5$ unit as calculated by $\bar{M}n_{,SEC}$), THT substrate (25 μL, 283.5 μmol) were dissolved in ACN (5 mL) at 25 °C under argon. The reaction were initiated by addition of 35% aqueous H_2O_2 (50 μL, 581.5 μmol) using a gas-tight syringe. The oxidation product were identified and quantified by HPLC using a C18 column (with a gradient temperature program).

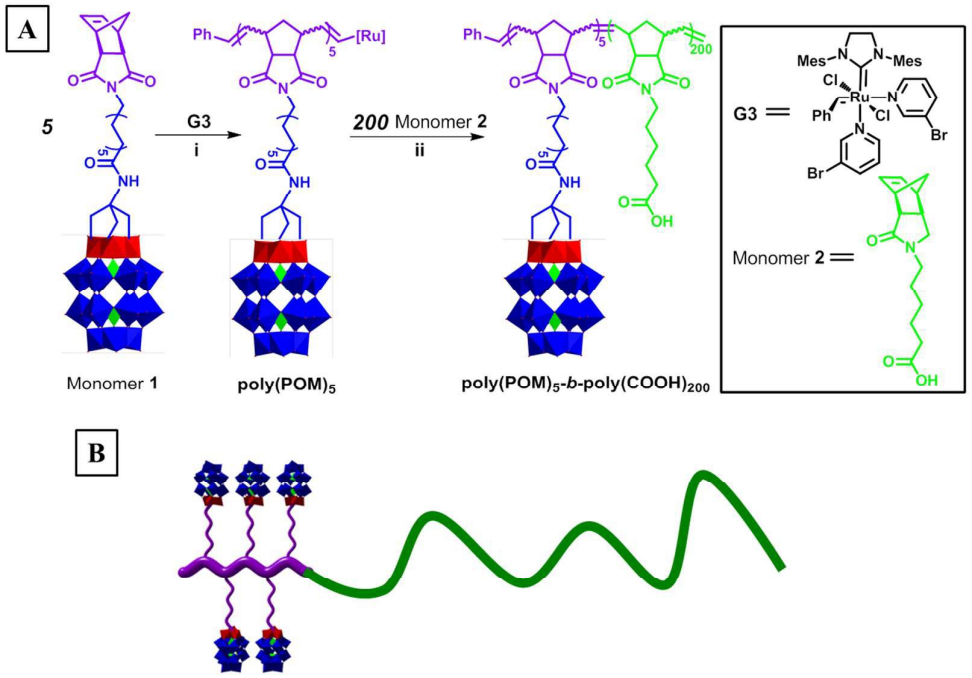

Scheme 1. Structure and synthesis of the designed poly(POM)$_5$-*b*-poly(COOH)$_{200}$

block copolymer. Reagents and conditions: (i) DMF, rt, 1 h. (ii) rt, 1h; then EVE (200 μL), rt, 10 min.

Results and discussion

Design and synthesis of H-BCP. Scheme 1 displays the structures of the two monomers and the hybrid block copolymer (H-BCP). Monomer **1** is a Wells-Dawson POM-containing norbornene monomer that was reported in the previous study.[37] Monomer **2** is a hexanoic acid-containing norbornene monomer. We selected a carboxyl as side group-containing monomer because the carboxyl-containing monomer can be dissolved in polar aprotic solvent dimethylformamide (DMF) that was used for the preparation of the linear poly(POM)s.[37] The polymer of the carboxyl-containing monomer is denoted as poly(COOH). Thus the H-BCP is denoted as poly(POM)$_m$-*b*-poly(COOH)$_n$. Considering the large size differences between the two monomers[45,46] and molecular weight (5833 Da of **1** versus 277 Da of **2**), we designed the H-BCP with a degree of polymerization m = 5 for the poly(POM) block and n = 200 for the poly(COOH) block, that is, poly(POM)$_5$-*b*-poly(COOH)$_{200}$. The two blocks not only have differences in chemical structure and property but also asymmetries in molecular weight and length.

Scheme 1 also displays the synthetic route of the poly(POM)$_5$-*b*-poly(COOH)$_{200}$ in DMF. Because the POM cluster is encapsulated by six cationic tetrabutylammoniums (Bu_4N^+), the reaction can be performed in DMF. As shown in Scheme 1, the H-BCP was prepared via a one-pot two-step sequential ROMP procedure.[47-50] The first step is to polymerize **1** into poly(POM)$_5$ at a molar ratio [G3]/[M1] = 1:5 using Grubbs' 3rd catalyst (1 eq) and **1** (5 eq) in DMF solution and the second step is to add a DMF solution of monomer **2** (200 eq) into the living poly(POM)$_5$-catalyst and DMF mixture, *i.e.* at a molar ratio [G3]/[M1]/[M2] = 1:5:200.

The chemical structure of the H-BCP was carefully characterized by ^{1}H and ^{31}P NMR, and FT-IR. Its molecular weight was determined by SEC equipped with both refractive index and online light-scattering detectors. The full ^{1}H NMR spectra of **2**, poly(POM)$_5$ and H-BCP are summarized in the ESI†. In comparison with these

spectra, we see that the signals of vinyl protons of the norbornene monomer at δ = 6.30 ppm disappear after polymerization. This indicates that the monomers were converted into the polymers. The formation of the block copolymer can also be confirmed by analyzing the characteristic signals of the ^{1}H NMR spectra.

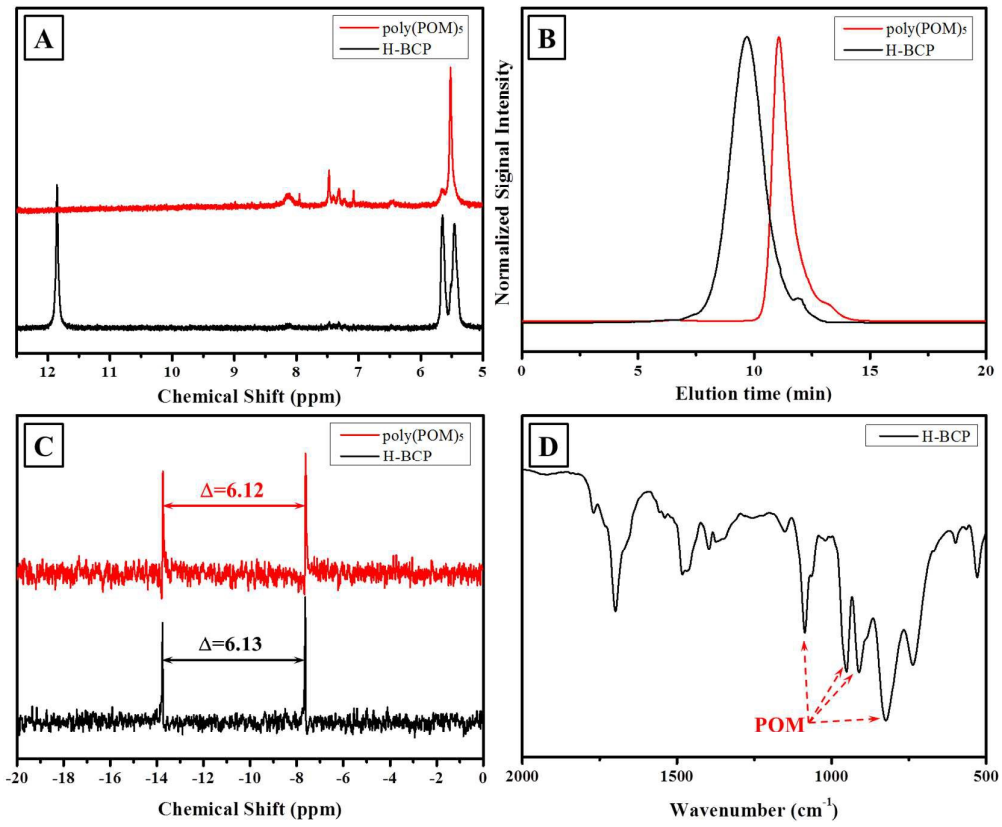

Fig. 1 ^{1}H NMR spectra (A), SEC traces (B) and ^{31}P NMR spectra (C) of the poly(POM)$_5$ and H-BCP. (D) FT-IR spectrum of the H-BCP.

Fig. 1A is the ^{1}H NMR spectra of the poly(POM)$_5$ and H-BCP from 5.00 to 12.50 ppm. The signals at 5.45 and 5.65 ppm are most important because they originate from the carbon-carbon double bond of the polynorbornene backbone. For the poly(POM)$_5$, the two signals are overlapped by the six tris-methylene protons. Weak signals at 7.00 to 8.20 ppm correspond to the protons of the amide and phenyl group. The H-BCP also shows two signals at 5.45 and 5.65 ppm with a ratio of 1.2/1.0 and a weak peak at 7.47 ppm. Importantly, a strong signal at 11.85 ppm corresponds to the carboxyl proton. It indicates that **2** was initiated by the catalytic active sit at the end of the poly(POM)$_5$ chain and further extended into poly(POM)$_5$-*b*-poly(COOH)$_{200}$.

The molecular weight study is another efficient method to confirm the formation of block copolymers. Two normalized SEC traces in Fig. 1B show the monomodal molecular weight distributions of the poly(POM)$_5$ and H-BCP. We note that their absolute weight-average molecular weights, $\bar{M}_{\mathrm{w,SEC}}$ were obtained because the online light-scattering detector was used. Table 1 summarizes the molecular weights and polydispersities of the poly(POM)$_5$ and H-BCP. Their polydispersity indexes (PDIs) are PDI ≤ 1.21 reflecting the typical characteristics of living ROMP. The number-average degrees of polymerization, $\overline{DP}_{\mathrm{SEC}}$, of each block are $\overline{DP}_{\mathrm{SEC}}$= 4.9 for the poly(POM) block that is nearly the same as the theoretical value ($\overline{DP}_{\mathrm{Theo}}$=5) and $\overline{DP}_{\mathrm{SEC}}$ = 232 of the poly(COOH) block that is slightly larger than $\overline{DP}_{\mathrm{Theo}}$ = 200. This difference is possibly due to the effect of withdrawing a small amount of the poly(POM) precursor for characterization. These suggest almost complete monomer-to-polymer conversions to form the poly(POM)$_5$ block and then the poly(COOH)$_{232}$ block via the living ROMP.

Table 1. Feed ratios of the poly(POM)$_5$ and H-BCP and their degrees of polymerization, molecular weights and polydispersities.

Samples	[G3]/[M1]/[M2][a]	$\overline{DP}_{\mathrm{SEC}}$ [b]	$\bar{M}_{\mathrm{n,Theo}}$ (kDa)[c]	$\bar{M}_{\mathrm{n,SEC}}$ (kDa)[d]	$\bar{M}_{\mathrm{w,SEC}}$ (kDa)[e]	PDI[f]
poly(POM)$_5$	1:5	4.9	29.3	28.4	32.9	1.16
H-BCP	1:5:200	4.9:232	84.7	92.7	112.0	1.21

[a][G3]:[M1]:[M2] means the molar ratio of the Grubbs' 3rd catalyst, monomer **1** and monomer **2**; [b]the degree of polymerization of poly(POM)$_5$ and H-BCP calculated by $\bar{M}_{\mathrm{n,SEC}}$; [c]the theoretical number-average molecular weight; [d]the number-average molecular weight measured by SEC; [e]the weight-average molecular weight measured by SEC; and [f]calculated by $\bar{M}_{\mathrm{w,SEC}}/\bar{M}_{\mathrm{n,SEC}}$.

The structural stability and integrity of POM clusters are still major concerns in their organic functionalization. In this work, we performed ^{31}P NMR and FT-IR characterizations to confirm the intactness of the POM cluster during polymerization of the two monomers into poly(POM)$_5$-*b*-poly(COOH)$_{232}$. Fig. 1C is the ^{31}P NMR spectra of the poly(POM)$_5$ and H-BCP. The two signals at δ = −7.63 and −13.76 ppm correspond to the two phosphorus heteroatoms residing at different positions of this POM cluster.[42] The negligible difference between the poly(POM)$_5$ (Δ = 6.12) and

H-BCP (Δ = 6.13) shows that the POM clusters remain unchanged after the poly(POM)$_5$ macro-catalyst triggered the polymerization of **2**. Meanwhile, the FT-IR characterization of the H-BCP exhibits the characteristic infrared signals of the POM clusters at v = 1086, 954, 910 and 824 cm^{-1} (Fig. 1D).[42] These analyses highlight the structural intactness of the POM cluster in the H-BCP. Therefore, we can conclude that we have synthesized the first poly(POM)$_5$-*b*-poly(COOH)$_{232}$ block copolymer with a relatively narrow molecular weight distribution by living ROMP. Importantly, the solid sample that was prepared from its DMF solution can be deformed without fracture, and thus exhibits good ductility (Fig. S6 in the ESI†).

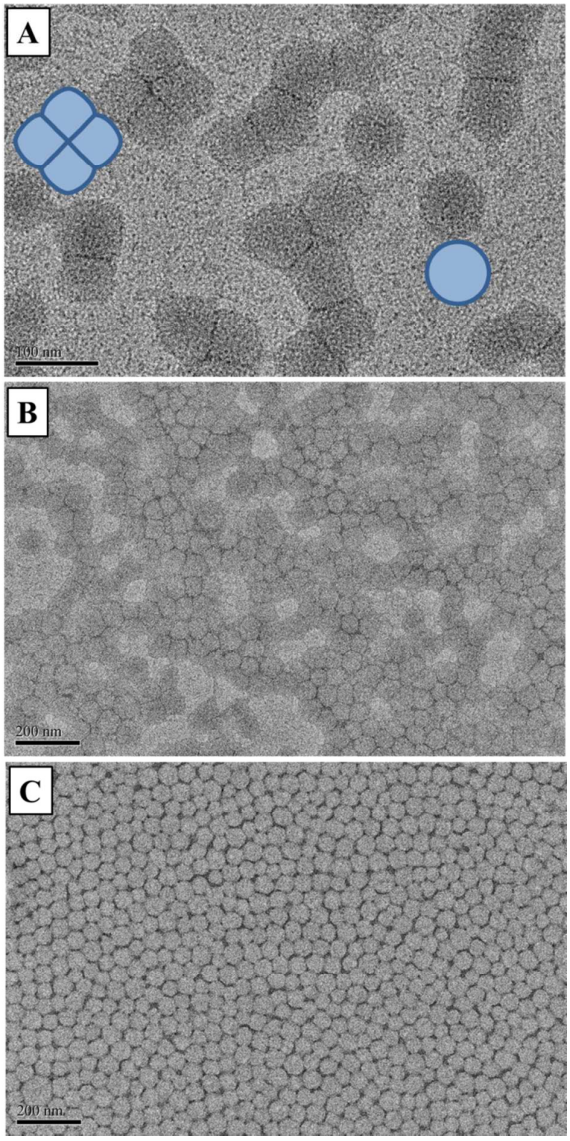

Fig. 2 TEM images of the H-BCP obtained from its ACN solution-cast samples. (A)

Isolated and clustered aggregates; (B) Networked ones; (C) Close-packed ones. The isolated aggregates are spheres, the clustered ones are deformed spheres and close-packed ones are irregular polygons. The schematic drawings in A represent ideal features of an isolated aggregate and a four-aggregate cluster.

Self-Assembled Micelles. The pure poly(POM)$_5$ can be well dissolved in anhydrous acetonitrile (ACN) at room temperature whereas the poly(COOH)$_{232}$ homopolymer can be swollen in the same solvent at 60 °C. This difference in solubility is used to create supramolecular aggregates in ACN. In the experiment, a transparent ACN solution of the H-BCP at a concentration of c = 2.0 mg/mL was prepared at 60 °C. When the hot solution was cooled to room temperature and then stood for 6 hours, it became turbid and exhibited strong Tyndall effect. TEM was used to characterize the resulting aggregates. The TEM samples were prepared by dropping 10 μL of the solution onto carbon-supported grids. Most ACN was quickly removed using a piece of filter paper and residual ACN was further removed in a vacuum oven at 25°C.

We observed many isolated, clustered and close-packed aggregates in thin films. The TEM images in Figs. 2A-C show the morphological features that we found in areas on the edge (A), between the edge and center (B) and in the center of the film (C). These aggregates may be spheres (S), deformed spheres (DS) or irregular polygons (IP). Two S-aggregates are deformed into two DS-aggregates when they contact each other. An S-aggregate is deformed into an IP-aggregate when it contacts with more than two neighboring ones. We used their average areas S to evaluate their size due to their shape uncertainty.

Fig. 2A shows isolated S-aggregates and clustered aggregates that are composed of two to five DS-aggregates. The average area of the individual aggregates in Fig. 2A is S = 4839 ± 403 nm^2 (Fig. S7 in the ESI†). If we carefully inspect the isolated S-aggregates, we can see a slightly darker ring, shown schematically by a circular drawing. This suggests that the electron density of the ring is slightly higher than the center. The boundaries between the two DS-aggregates become straight and darker and the intersection points of three or four DS-aggregates are much darker. The

average area of these DS-aggregates decreases with increasing contact number. These features are schematically depicted in Fig. 2A.

The TEM image in Fig. 2B shows a morphological feature in which many DS- and IP-aggregates gather to form large clusters or even a network. The measured average area is $S = 3236 \pm 547$ nm^2 (Fig. S8 in the ESI†), which is smaller than that in Fig. 2A. In the center of the thin film sample we found close-packed aggregates (Fig. 2C). The darker boundary becomes thicker. We see better contrast between the boundary, intersection points and center of the IP-aggregates. Thus, we can easily identify the shapes of individual aggregates as dominant hexagons and a few irregular polygons with five or seven sides. The measured average area is $S = 2150 \pm 381$ nm^2 (Fig. S10 in the ESI†), which is the smallest in the three observation areas. These analyses suggest that the aggregate size decreases and its size distribution increases from the edge to the center of the thin film sample. These results are similar to that found in foam. Thus, we believe that the aggregates should be soft in solution as well as on the carbon film during solvent evaporation.

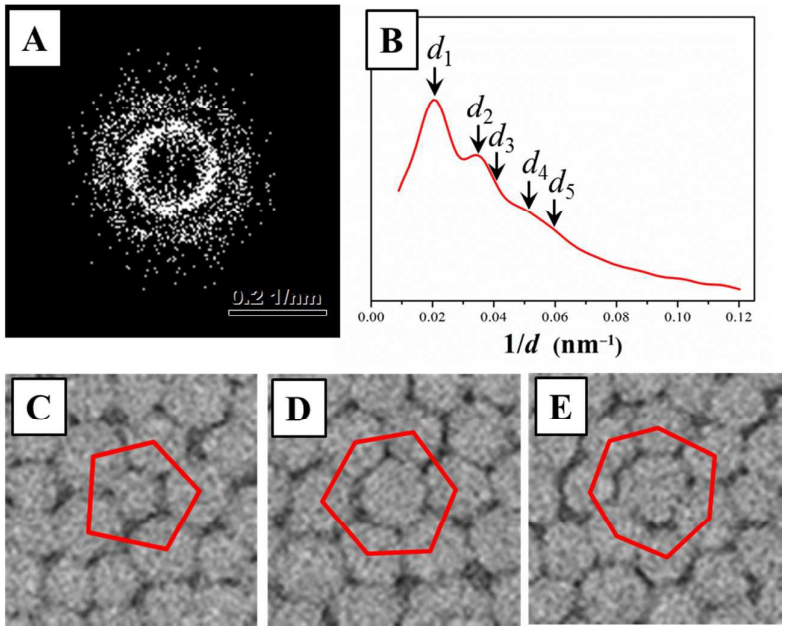

Fig. 3 (A) 2D FFT pattern corresponding to the TEM image in Fig. 2C. (B) Digital 1D FFT pattern corresponding to (A). Arrows indicate the peaks. (C) to (E) Pentagonal, hexagonal and heptagonal close-packed aggregates highlighted by an irregular pentagon, hexagon and heptagon, respectively.

Fig. 3A is a two-dimensional (2D) fast Fourier transform (FFT) pattern with two identifiable rings that corresponds to the structure in Fig. 2C. The contrast of the pattern was enhanced for better presentation. Fig. 3B is a plot of brightness intensity in Fig. 3A versus reciprocal length ($1/d$) obtained by azimuthally integrating the 2D FFT pattern. The plot shows four identifiable peaks and a shoulder peak as indicated by arrows in Fig. 3B. The broad peaks and their ratio of $d_5/d_4/d_3/d_2/d_1 \approx 3/\sqrt{7}/2/\sqrt{3}/1$ suggest a hexagonal close-packed (HCP) structure of the IP-aggregates but not perfect. The average distance between the two neighboring aggregates is $d \approx 49.5$ nm.

In Fig. 3C to 3E we highlight three irregularly pentagonal, hexagonal and heptagonal close-packed structures that are found in Fig. 2C. Of these, the irregular HCP is the most popular one. This is the reasons why our statistical analysis in Fig. 3B presents a HCP structure (Fig. 3C). Furthermore, the size differences in the IP-aggregates in Figs. 3C to 3E are very interesting. The smallest IP-aggregate is in the center of the pentagonal close-packing (Fig. 3C), while the largest IP-aggregate stands in the center of the heptagonal close-packing (Fig. 3E). The seven IP-aggregates in the hexagonal close-packing have a uniform size that is close to the average value (Fig. 3D). Finally, we find two rules: 1) the number of the sides of an IP-aggregate equals the number of the aggregates on the periphery; 2) a long side corresponds to a large neighboring aggregate.

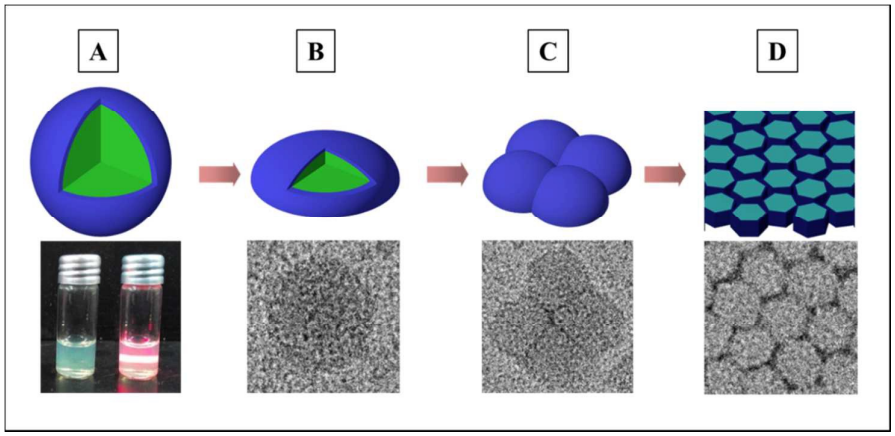

Fig. 4 The drawings are proposed models of spherical aggregates in solution, and flattened, clustered and close-packed aggregates in thin films. These drawings also describe the process from spherical aggregates to close-packed aggregates during

solvent evaporation. The optical picture shows a turbid solution with the Tyndall effect and the TEM pictures present the typical morphologies.

Here, we propose models to describe the structure of the aggregates in solution and the structural evolution from isolated aggregates to close-packed ones during solvent evaporation. In Fig. 4A a core-shell micelle model is suggested to depict the supramolecular structure of the aggregates formed in the ACN solution of the H-BCP. The poly$(POM)_5$ block forms shell and the poly$(COOH)_{232}$ block forms core because of the better solubility of the poly(POM) block. In this way, the solution becomes turbid and exhibits strong Tyndall effect (see the pictures in Fig. 4A).

Fig. 4B presents a model of flattened micelles to describe the isolated aggregates found in our TEM study (see the TEM image in Fig. 4B). This is because the ACN-swollen micelles are soft and thus flattened during the solvent evaporation. This is the reason why the flattened micelles have weak contrast between the shell and core under TEM observation.[51]

Figs. 4C and 4D represent the proposed models of a four-micelle cluster and of close-packed micelles, respectively. Their formation is driven by the attractive capillary forces between the micelles caused by solvent evaporation.[52] During this process, the soft micelles are squeezed and thus deformed. Thus, the size of the deformed micelles is smaller than that of the isolated ones. Normally, micelles prefer to arrange hexagonally because HCP is one of the densest possible packings of equal spheres. The wide size distribution of the micelles leads to the formation of the pentagonal and heptagonal close-packings (Figs. 3C and 3E). These analyses suggest that Fig. 4 also presents the process of the structural evolution from isolated to hexagonal close-packed micelles during solvent evaporation.

Catalytic activity and kinetics. Catalytic activity of POMs is one of the important functions in practical application. For instance, they can catalyze the oxidation of sulfur-containing compounds. Therefore, we appraised the catalytic activity of the H-BCP as well as the poly$(POM)_5$ homopolymer in the catalytic

oxidation of tetrahydrothiophene (THT), which is a well-known gasoline contaminant, into tetrahydrothiophene oxide (THTO). The oxidative desulfurization experiments were performed in an ACN (5 mL) solution of THT (25 μL) and the H-BCP or poly(POM)$_5$ catalyst (10.0 mg) at 25 °C.[37] The catalytic oxidation of THT was initiated when 35% aqueous H_2O_2 (50 μL) was added to the solution.

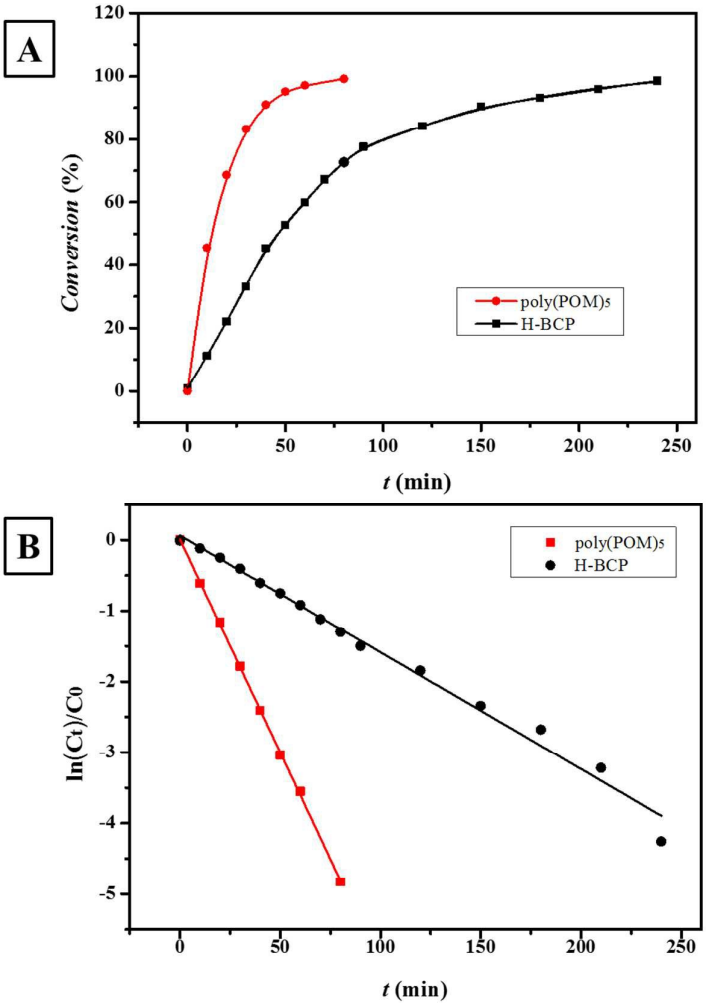

Fig. 5 Plots of conversion (A) and ln(C_t/C_0) (B) *versus* the reaction time, *t*, for the oxidation of tetrahydrothiophene (THT) into tetrahydrothiophene oxide (THTO) catalyzed by the H-BCP and poly(POM)$_5$ homopolymer.

Fig. 5A shows conversion-time plots of the THTO catalyzed by the H-BCP and poly(POM)$_5$. Clearly, the POM clusters in the poly(POM)$_5$ shell in the H-BCP micelles can catalytically oxidize THT into THTO. The conversion α = 90% was reached at *t* ≈ 150 min for the H-BCP, however, α = 90% at *t* ≈ 40 min for the

poly(POM)$_5$ homopolymer under the same conditions. Apparently, the catalytic efficiency of the poly(POM)$_5$ shell in the H-BCP micelles is lower than the poly(POM)$_5$ homopolymer.

We further evaluated the catalytic reaction kinetics. Fig. 5B shows plots of $\ln(C_t/C_0)$-t for the oxidation of THT into THTO, in which C_0 and C_t correspond to initial THT concentration and its concentration at time t, respectively. Because the concentration of H_2O_2 did not change too much during the catalytic reactions, it could be regarded as a constant. Therefore, the reaction kinetics can be described by

$$\ln(C_t/C_0) = -kt \quad (1)$$

where k is the reaction rate constant. In Fig. 5B, the good linear relations between $\ln(C_t/C_0)$ and t reveal that the oxidation reaction, catalyzed by both the H-BCP and poly(POM)$_5$, exhibits pseudo-first-kinetics.[53–55] The reaction rate constants obtained from the slopes are k = –0.0603 min^{-1} for poly(POM)$_5$ and k = –0.0168 min^{-1} for the H-BCP, respectively. Thus, the rate constant ratio of the reactions catalyzed by two catalysts is about 3.6. This result again indicates that the catalytic efficiency of the poly(POM)$_5$ in the H-BCP is lower than the poly(POM)$_5$ homopolymer. There are two reasons for this: First, the H-BCP forms micelles that is a heterogeneous catalyst and second, the catalytic units in the H-BCP (0.11 μmol, 1 eq) are nearly one third of the poly(POM)$_5$ homopolymer (0.35 μmol, 3.2 eq) under the same mass concentration.

Conclusions

In summary, a poly(polyoxometalate)-polymer hybrid block copolymer (H-BCP) with a controllable molecular weight and a low polydispersity was prepared by ROMP. In acetonitrile, the H-BCP self-assembles into hybrid micelles with a POM-containing shell and an organic polymer core. When casting thin films, the micelles further self-assemble into a hexagonal close-packed structure driven by the attractive capillary forces between the micelles due to solvent evaporation. Meanwhile, the POM clusters within the H-BCP present good oxidation catalytic

activity. This means that it may be used as a heterogeneous catalyst. Compared with the homo-poly(polyoxometalate)s developed in our previous work,[37] the hybrid block copolymer demonstrates varied self-assembled structures and improved performance and functionality. We believe that this approach is very promising for the construction of functional POM-containing hybrid materials with good processability and durability.

Acknowledgment

We appreciate the financial support of the National Natural Science Foundation of China for grants (NSFC 21274069 and 21334003), PCSIRT (IRT1257), and Open Research Fund of State Key Laboratory of Polymer Physics and Chemistry, Changchun Institute of Applied Chemistry.

Notes and references

1 Special thematic issue on hybrid materials. *Chem. Soc. Rev.*, 2011, **40**, 471–1150.
2 M. C. Orilall and U. Wiesner, *Chem. Soc. Rev.* 2011, **40**, 520–35.
3 C. Laberty-Robert, K. Valle, F. Pereira and C. Sanchez, *Chem. Soc. Rev.*, 2011, **40**, 961–1005.
4 B. Lebeau and P. Innocenzi, *Chem. Soc. Rev.*, 2011, **40**, 886–906.
5 M. Vallet-Regi, M. Colilla and B. Gonzalez, *Chem. Soc. Rev.*, 2011, **40**, 596–607.
6 J. Yuan, Y. Xu and A. H. Müller, *Chem. Soc. Rev.*, 2011, **40**, 640–655.
7 R. Pardo, M. Zayat and D. Levy, *Chem. Soc. Rev.*, 2011, **40**, 672–87.
8 G. Kickelbick, *Prog. Polym. Sci.*, 2003, **28**, 83–114.
9 G. Kickelbick, *Hybrid Materials: Synthesis Characterization, and Applications;* Wiley-VCH: Weinheim, 2007.
10 G. González-Moraga, *Cluster Chemistry: Introduction to the Chemistry of Transition Metal and Main Group Element Molecular Clusters*; Springer-Verlag: Berlin and Heidelberg, 1993.
11 U. Schubert, *Chem. Mater.*, 2001, **13**, 3487–3494.
12 X.-F. Yu, Y.-W. Li, X.-H. Dong, K. Yue, Z.-W. Lin, X.-Y. Feng, M.-J. Huang, W.-B. Zhang and S. Z. D. Cheng, *J. Polym. Sci. Polym. Phys.*, 2014, **52**, 1309–1325.
13 M. Pope and A. Müller, *Polyoxometalate chemistry from topology via self-assembly to applications*; Springer Science & Business Media, 2001.
14 Special thematic issue on polyoxometalates and their applications. *Chem. Rev.*, 1998, **98**, 1–388.
15 W. Qi and L.-X. Wu, *Polym. Intern.*, 2009, **58**, 1217–1225.
16 P. Judeinstein, *Chem. Mater.*, 1992, **4**, 4–7.
17 C. R. Mayer, V. Cabuil, T. Lalot and R. Thouvenot, *Angew. Chem. Int. Ed.*, 1999, **38**, 3672–3675.
18 C. R. Mayer and R. Thouvenot, *Chem. Mater.*, 2000, **12,** 257–260.

19 C. R. Mayer and R. Thouvenot, *Macromolecules*, 2000, **33**, 4433–4437.
20 J. L. Horan, A. Genupur, H. Ren, B. J. Sikora, M.-C. Kuo, F. Meng, S. F. Dec, G. M. Haugen, M. A. Yandrasits, S. J. Hamrock, M. H. Frey and A. M. Herring, *ChemSusChem*, 2009, **2**, 226–229.
21 A. R. Moore, H. Kwen, A. M. Beatty and E. A. Maatta, *Chem. Commun.*, 2000, 1793–1794.
22 H.-L. Li, W. Qi, W. Li, H. Sun, W. Bu and L.-X. Wu, *Adv. Mater.*, 2005, **17**, 2688–2692.
23 L. Xu, M. Lu, B.-B. Xu, Y.-G.Wei, Z.-H. Peng and D. R. Powell, *Angew. Chem. Int. Ed.*, 2002, **41**, 4129–4132.
24 M. Lu, B. Xie, J. Kang, F. Chen, Y. Yang and Z.-H. Peng, *Chem. Mater.*, 2005, **17**, 402–408.
25 B. Xu, M. Lu, J. Kang, D. Wang, J. Brown and Z.-H. Peng, *Chem. Mater.*, 2005, **17**, 2841–2851.
26 S. Chakraborty, A. Keightley, V. Dusevich, Y. Wang and Z.-H. Peng, *Chem. Mater.*, 2010, **22**, 3995–4006.
27 Y.-K. Han, Y. Xiao, Z.-J. Zhang, B. Liu, P. Zheng, S.-J. He and W. Wang, *Macromolecules*, 2009, **42**, 6543–6548.
28 N. Xia, W. Yu, Y.-L. Wang, Y.-K. Han, P. Zheng, W. Wang, G. Sakaguchi, K. Matsuda, K. Saijo, M. Takenaka and H. Hasegawa, *Polymer*, 2011, **52**, 1772–1780.
29 Y.-K. Han, Z.-J. Zhang, Y.-L. Wang, N. Xia, B. Liu, Y. Xiao, L.-X. Jin, P. Zheng and W. Wang, *Macro. Chem. Phys.* 2011, **212**, 81–87.
30 Y. Xiao, Y.-K. Han, N. Xia, M.-B. Hu, P. Zheng and W. Wang, *Chem. Eur. J.* 2012, **18**, 11325–11333.
31 J. Rieger, T. Antoun, S.-H. Lee, M. Chenal, G. Pembouong, J. L. de la Haye, I. Azcarate, B. Hasenknopf and E. Lacôte, *Chem. Eur. J.* 2012, **18***,* 3355–3361
32 J. L. de la Haye, A. P. da Costa, G. Pembouong, L. Ruhlmann, B. Hasenknopf, E. Lacôte and J. Rieger, *Polymer*, 2015, **57**, 173–182;
33 J. L. de la Haye, J.-M. Guigner, E. Marceau, L. Ruhlmann, B. Hasenknopf, E. Lacôte and J. Rieger, *Chem. Eur. J.*, 2015, **21**, 2948–2953.
34 M.-B. Hu, N. Xia, W. Yu, C. Ma, J. Tang, Z.-Y.; Hou, P. Zheng and W. Wang, *Polym. Chem.*, 2012, **3**, 617–620.
35 J. Tang, W. Yu, M.-B. Hu, Y Xiao, X.-G. Wang, L.-J. Ren, P. Zheng, W. Zhu, Y. Chen and W. Wang, *ChemPlusChem*, 2014, **79**, 1455–1462.
36 J. Tang, C. Ma, X.-Y. Li, L.-J. Ren, H. Wu, P. Zheng and W. Wang, *Macromolecules*, 2015, **48**, 2723−2730..
37 W.-K. Miao, Y.-K. Yan, X.-L. Wang, Y. Xiao, L.-J. Ren, P. Zheng, C.-H. Wang, L.-X. Ren and W. Wang, *ACS Macro Lett.*, 2014, **3**, 211–215.
38 I. W. Hamley, Block Copolymers in Solution: Fundamentals and Applications, *John Wiley & Sons, Ltd,* Chichester, 2007.
39 I. W. Hamley, The Physics of Block Copolymers, Oxford University Press, Oxford, 1998.
40 J. A. Love, J. P. Morgan, T. M. Trnka and R. H. Grubbs, *Angew. Chem. Int. Ed.*,

2002, **41**, 4035−4037.

41 R. G. Finke, B. Rapko, R. J. Saxton and P. J. Domaille, *J. Am. Chem. Soc*., 1986, **108**, 2947−2960.

42 Y. Hou, C. L. Hill, *J. Am. Chem. Soc.*, 1993, **115**, 11823−11830.

43 The IUPAC nomenclature of the monomer is 6-(3,5-Dioxo-4-azatricyclo[5.2.1.$0^{2\text{-}exo,6\text{-}exo}$]-dec-8-en-4-yl) hexanoic acid.

44 I. N. Tarabara, Y. S. Bondarenko and L. I. Kas'yan, *Russ. J. Org. Chem.*, 2009, **45**, 234−241.

45 This POM cluster has an ellipsoid shape with a long axis of 1.2 nm and a short axis of 1.0 nm.

46 C. P. Pradeep, D. L Long, G. N. Newton, Y. F. Song and L. Cronin, *Angew. Chem. Int. Ed*., 2008, **47**, 4388−4391.

47 L. Ren, J. Zhang, C. G. Hardy, S. Ma and C. B. Tang, *Macromol. Rapid Commun.*, 2012**, 33**, 510–516.

48 L. X. Ren, J. Y. Zhang, X. L. Bai, C. G. Hardy, K. D. Shimizu and C. B. Tang, *Chem. Sci.*, 2012, **3**, 580−583.

49 Y.-P. Zha, H. D. Thaker, R. R. Maddikeri, S. P. Gido, M. T. Tuominen and G. N. Tew, *J. Am. Chem. Soc.*, 2012, **134**, 14534−14541.

50 Z.-L. Li, L. Li, F.-S. Du and Z.-C. Li, *Chin. J. Polym. Sci.*, 2013, **31**, 355−362.

51 M. Yang, W. Wang, F. Yuan, X.-W. Zhang, J.-Y. Li, H.-X. Liang, B.-L. He, B. Minch and G. Wegner, *J. Am. Chem. Soc.*, 2005, **127**, 15107–15111.

52 Y.-J. Min, M. Akbulut, K. Kristiansen, Y. Golan and J. Israelachvili, *Nat. Mater.*, 2008, **7**, 527−538.

53 M. V. Vasylyev and R. Neumann, *J. Am. Chem. Soc.*, 2004, **126**, 884–890.

54 A. Nisar, J. Zhuang and X. Wang, *Adv. Mater.*, 2011, **23**, 1130–1135.

55 Y. Xiao, D. Chen, N. Ma, Z.-Y. Hou, M.-B. Hu, C.-H. Wang and W. Wang. *RSC Advances*, 2013, **3**, 21544-21551.